New ideally absorbing Au plasmonic nanostructures for biomedical applications

Vadim I. Zakomirnyi[a], Ilia L. Rasskazov[a,*], Sergey V. Karpov[a,b,c], Sergey P. Polyutov[a]

[a]*Siberian Federal University, 660041 Krasnoyarsk, Russia*
[b]*L. V. Kirensky Institute of Physics, 660036 Krasnoyarsk, Russia*
[c]*Siberian State Aerospace University, 660037 Krasnoyarsk, Russia*

Abstract

In this paper a new set of plasmonic nanostructures operating at the conditions of an ideal absorption [1] was proposed for novel biomedical applications. We consider spherical x/Au nanoshells and Au/x/Au nanomatryoshkas, where 'x' changes from conventional Si and SiO_2 to alternative plasmonic materials [2], such as zinc oxide doped with aluminum, gallium and indium tin oxide. The absorption peak of proposed nanostructures lies within 700-1100nm wavelength region and corresponds to the maximal optical transparency of hemoglobin and melanin as well as to the radiation frequency of available pulsed medical lasers. It was shown that the ideal absorption takes place in a given wavelength region for Au coatings with thickness less than 12nm. In this case finite quantum size effects for metallic nanoshells play significant role. The mathematical model for the search of the ideal absorption conditions was modified by taking into account the finite quantum size effects.

Keywords: ideal absorption, plasmonic photothermal therapy, nanoshell, nanomatryoshka

1. Introduction

In last decades metallic nanoparticles have attracted significant attention due to their ability to localize the electromagnetic energy on a scale much smaller than the wavelength of incident radiation [3–5]. Absorption of radiation is significantly enhanced at the frequency of the nanoparticle surface plasmon resonance. Biomedicine and biotechnology probably are one of the most promising applications of plasmonic nanoparticles [6–22].

Bio-compatibility and ability to conjugate with biomacromolecules are important properties of gold nanoparticles. These features make gold the best plasmonic material for biomedical applications. Biological systems based on plasmonic nanoparticles make it possible to employ them in early diagnostics, therapy as well as in medical imaging and monitoring of the treatment of malignant neoplasms.

Plasmonic photothermal therapy (PPTT) [23–32] is one of the important biomedical application of plasmonic nanoparticles which represents the thermally selective impact of laser radiation on malignant tissue labeled by plasmonic nanoparticles.

*Corresponding author
Email address:* `il.rasskazov@gmail.com` (Ilia L. Rasskazov)

This approach is one of promising tools in oncology which is developed over the last decade. It has had some success in treating cancer in last years and offers important advantages over conventional therapies. PPTT is probably the one possible treatment of locally invasive, unresectable and refractory to chemotherapy and radiation therapy tumors. Therefore, PPTT has a great therapeutic potential to target locally advanced disease which has become resistant to conventional and standard treatments. This strategy has, however, several limitations in clinical settings. A general concern is its potential toxicity on the human body, the delivery of nanoparticles and light into tissue, contrast of therapy and immune response. However last researches reached success in solving these problems.

Highly accurate delivery of nanoparticles to a biological target can be attained via biological conjugates "nanoparticle-aptamer" [33, 34]. Such conjugates of plasmonic nanoparticles with adsorbed on their surface the synthetic oligonucleotides (deoxyribonucleic acid (DNA) aptamers) provide functionalization of these complexes. As a consequence, aptamers bound highly specifically with fragments of proteins (tumor markers), located only on the membrane of malignant cells. Au nanoparticles related to DNA aptamers interact with the laser radiation in the plasmonic absorption band and heat local area around a tumor rising its temperature up to 42-43°C and higher. It induces apoptosis of malignant cells (controlled cell death process). Moreover, such Au bioconjugates have low toxicity, which is particularly important when they are used in complex therapy of oncological diseases.

The use of Au nanoparticles in PPTT is also promising due to controllable delivery of laser radiation into tissue. Initial efforts with spherical nanoparticles [35–37], however, were not very effective in vivo because for homogeneous Au spherical nanoparticles absorption peak corresponds to 500-600nm wavelength region. These wavelengths lie beyond a biological transparency window. Therefore, spherical nanoparticles can hardly be used in PPTT of skin or near-surface type cancers due to inability of the visible light to penetrate through skin and tissue. Solution of this problem is associated with the developing of Au nanoparticles having absorption peak lying within the biological transparency window. The absorption peak of Au nanorods [11, 25, 26, 38] may be tuned from 550 nm up to 1μm by altering its aspect ratio. Another way is to utilize Au nanoshells with a high refractive index of core material (e.g., Si or SiO_2) [23, 39–43]. The absorption peak of Au nanoshells is easily tuned to biological transparency window by varying both core radius and shell thickness. Recently it was shown that Au multilayered nanoparticles (nanomatryoshkas) with intermediate SiO_2 layer are also promising candidates for PPTT [32, 44]. Finally, various alternative geometries of nanoparticles, such as nanocages [45], nanostars [46] and hollow spheres [47] have been also considered in literature.

It is obvious, that the faster and higher heating effects in PPTT make it possible to use moderate or even low intensity laser radiation for highly efficient damage of malignant cells. Under these conditions, the destructive consequences for normal tissue are significantly reduced. Therefore, there is an advantage to incorporate effectively absorbing nanopar-

ticles into the PPTT. For example, there are different theoretical and experimental approaches to optimize absorbing properties of Au spheres [48] or Au nanorods [38, 49]. However, in our paper, we propose to utilize ideally absorbing two- and three-layered spherical nanoparticles for application with the PPTT method. Ideal absorption (IA) corresponds to the conditions of absorption of the radiation energy by the nanoparticle is close to theoretical maximum. There is an increasing interest to this topic in last few years [50–53]. To determine IA conditions we use conceptual ideas proposed in the recent paper [1]. The advantage of this approach is that it provides us with analytic expressions which allow one to find the optimal geometry of homogeneous or multi-layered nanospheres to reach the ideal absorption conditions. In order to fit the biological transparency window, one should use Au nanoshells with a thickness below 10nm. In this case, quantum size effects (QSE) for metallic nanoshells play a crucial role [18, 43, 54] and the method described in Ref. [1] loses accuracy. Therefore, the generalization of previously determined design formulas [1] for obtaining ideal absorption in core-shell configurations of the plasmonic material constituents with taking into consideration QSE is of considerable interest.

Additionally, in this paper we propose to examine Au nanoshells with the core consisting of the alternative plasmonic materials, including zinc oxide (ZnO), ZnO doped with aluminum or gallium (AZO and GZO, respectively) and indium tin oxide (ITO). Physical properties and applications of these materials in plasmonics are discussed recently [2, 55–57].

Therefore, in this paper we develop the algorithm for finding optimal geometry of ideally absorbing Au nanoparticles taking into account QSE and investigate the possibility of PPTT applications of two- and three-layered Au nanoparticles with core or intermediate layers consisting of alternative plasmonic materials.

2. Model

2.1. Optical Properties of Layered Nanoparticle

Consider a multilayered nanoparticle with an outer radius R embedded in a homogeneous environment with the dielectric permittivity ε_{b} (Fig. 1a,c). Each layer of nanoparticle is described by thickness l_i and dielectric permittivity ε_i. For the first layer (i.e., core), l_1 equals to its radius. We use the dipole equivalence principle described in detail in Refs [18, 20] to characterize the optical properties of multilayered nanoparticle.

In accordance to this principle, the multilayered nanoparticle with an outer radius R can be replaced by the equivalent homogeneous nanoparticle with the same radius R embedded into the same surrounding medium. If we assume that dipole moments induced on initial and equivalent nanoparticles are equal, then the equivalent dielectric permittivity $\varepsilon_{\mathrm{av}}$ of homogeneous nanopartilce can be easily found. Thus, for homogeneous sphere (Fig. 1b) that replaces two-layered nanoparticle (Fig. 1a) we have:

$$\overline{\varepsilon}_{\mathrm{av}}^{(2)} = \overline{\varepsilon}_2 \left[\frac{\overline{\varepsilon}_1 + 2\overline{\varepsilon}_2 + 2f_{12}(\overline{\varepsilon}_1 - \overline{\varepsilon}_2)}{\overline{\varepsilon}_1 + 2\overline{\varepsilon}_2 - f_{12}(\overline{\varepsilon}_1 - \overline{\varepsilon}_2)} \right], \quad (1)$$

where $f_{12} = [l_1/(l_1 + l_2)]^3$ is the filling factor and $\overline{\varepsilon}_i = \varepsilon_i/\varepsilon_{\mathrm{b}}$.
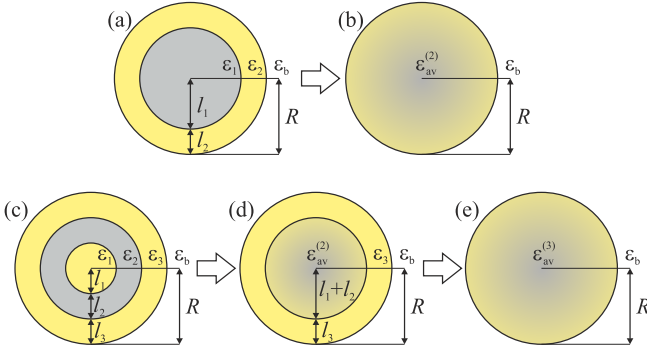
3

Figure 1: (Color online) Illustration of the dipole equivalence principle for two-layered nanoshell (top) and for three-layered nanomatryoshka (bottom): a) initial two-layered nanoshell; b) equivalent homogeneous sphere; c) initial three-layered nanomatryoshka; d) intermediate nanoshell; e) equivalent homogeneous sphere.

One of the advantage of dipole equivalence principle is that the above procedure can be recurrently repeated for any number of layers. In the case of three-layered nanomatryoshka (Fig. 1c) this scheme should be repeated twice. Firstly, we replace $i = 1$ and $i = 2$ layers with equivalent homogeneous core, so we obtain nanoshell (Fig. 1d). Then we replace such structure with homogeneous sphere (Fig. 1e) with equivalent dielectric permittivity:

$$\bar{\varepsilon}_{\mathrm{av}}^{(3)} = \bar{\varepsilon}_3 \left[\frac{\bar{\varepsilon}_{\mathrm{av}}^{(2)} + 2\bar{\varepsilon}_3 + 2 f_{23}(\bar{\varepsilon}_{\mathrm{av}}^{(2)} - \bar{\varepsilon}_3)}{\bar{\varepsilon}_{\mathrm{av}}^{(2)} + 2\bar{\varepsilon}_3 - f_{23}(\bar{\varepsilon}_{\mathrm{av}}^{(2)} - \bar{\varepsilon}_3)} \right], \quad (2)$$

where $\bar{\varepsilon}_{\mathrm{av}}^{(2)}$ is given by the eq. (1) and the filling factor $f_{23} = [(l_1 + l_2)/(l_1 + l_2 + l_3)]^3$.

2.2. Ideal Absorption

Recently it was shown [50, 51, 53] that theoretical absorption limit of surface plasmon resonances in spherical nanoparticles at free-space wavelength λ is given by:

$$\sigma_a = \frac{2n + 1}{8\pi\varepsilon_b} \lambda^2, \quad (3)$$

where σ_a is an absorption cross section, and n is the mode number. The electric dipole mode ($n = 1$) is predominant for Au nanopartilces with radius much smaller than wavelength λ. Thus, in our work we consider only dipole resonances and therefore, the absorption cross section of nanoparticle with ideal absorption should satisfy $\sigma_a = 3\lambda^2/8\pi\varepsilon_b$.

To determine the conditions for ideal absorption of nanoparticles we use the method proposed in Ref. [1]. This method provides explicit guidelines to search for size parameter $\rho = 2\pi\sqrt{\varepsilon_{\mathrm{b}}}R/\lambda$ and filling factors $f_{i,i+1}$ for multilayered nanoparticle with IA at a given wavelength λ. The dielectric permittivity of nanoparticle with IA must satisfy the following equation:

$$\bar{\varepsilon}_{\mathrm{IA}}(\rho) = \frac{1}{2}\frac{a^2}{b^2}\left[1 + \frac{\rho^2}{b^2}\frac{2(i\rho + 1)}{(\rho^2 - i\rho - 1)} - \right.$$
$$\left. - \sqrt{\left(1 + \frac{\rho^2}{b^2}\frac{2(i\rho + 1)}{(\rho^2 - i\rho - 1)}\right)^2 - \frac{\rho^2}{a^2}\frac{8(i\rho + 1)}{(\rho^2 - i\rho - 1)}} \right], \quad (4)$$

where $a = 1.4303\pi$ and $b = 0.87335\pi$.

In the case of two-layered nanoshell, the IA condition corresponds to equality $\bar{\varepsilon}_{\mathrm{av}}^{(2)}(f_{12}) = \bar{\varepsilon}_{\mathrm{IA}}(\rho)$ and the algorithm of search for optimal ρ and f_{12} values is as follows. Firstly, we obtain the expression for filling factor f_{12} from the eq. (1) and apply the IA condition:

$$f_{12} = \frac{\bar{\varepsilon}_1 + 2\bar{\varepsilon}_2}{\bar{\varepsilon}_1 - \bar{\varepsilon}_2}\frac{\bar{\varepsilon}_{\mathrm{IA}}(\rho) - \bar{\varepsilon}_2}{\bar{\varepsilon}_{\mathrm{IA}}(\rho) + 2\bar{\varepsilon}_2}. \quad (5)$$

Therefore, for fixed values of $\bar{\varepsilon}_i$ in eq. (5), f_{12} depends on ρ: $f_{12}(\rho)$. Taking into account that at least one of the dielectric permmitivities in the

4

eq. (5) is a complex parameter, it becomes obvious that in the general case, $f_{12}(\rho)$ is a complex too. Recall that $f_{12} = [l_1/(l_1 + l_2)]^3$ must be a real parameter. Secondly, from the plot of the function $f(\rho)$ we can define pairs $\{f_{12}, \rho\}$ that satisfy the condition $\mathrm{Im}\,[f(\rho)] \equiv 0$. Therefore one can define the geometry of two-layered nanoshells with IA at a given wavelength λ.

In the case of three-layered nanomatryoshkas the above algorithm becomes more complicated. We should define $\{f_{12}, f_{23}, \rho\}$ to describe the geometry of nanoparticle corresponding to the IA condition $\overline{\varepsilon}_{\mathrm{av}}^{(3)}(f_{12}, f_{23}) \equiv \overline{\varepsilon}_{\mathrm{IA}}(\rho)$. To implement it, we should have the expression for $f_{23} = f(f_{12}, \rho)$ from equations (1) and (2) and then find pairs of parameters $\{f_{12}, \rho\}$ complying with the condition $0 < f_{23} < 1$.

2.3. Finite-size effects

The above-stated algorithm for determining filling factors $f_{i,i+1}$ and size parameter ρ is accurate for multilayered spheres with relatively thick layers. However, in the case of thin layers we should take into consideration the quantum effects of finite size [54]. Tabulated values of ε_i should be replaced by the following correction:

$$\varepsilon_i \to \varepsilon_i + \frac{\omega_p^2}{\omega^2 + i\gamma_{\mathrm{bulk}}\omega} - \frac{\omega_p^2}{\omega^2 + i\gamma_{\mathrm{fin}}\omega}, \quad (6)$$

where $\omega = 2\pi c/\lambda$ is the frequency of incident radiation; ω_p is the plasma frequency; γ_{bulk} is the relaxation constant for a bulk and γ_{fin} is [54]:

$$\gamma_{\mathrm{fin}} = \gamma_{\mathrm{bulk}} + A_L \frac{v_{\mathrm{F}}}{L_{\mathrm{eff}}}, \quad (7)$$

where v_{F} is the Fermi velocity; L_{eff} is the mean free path of conduction electrons and A_L is the dimen-

sionless parameter, which is assumed to be close to unity in most of cases [58]. For gold $\gamma_{\mathrm{bulk}}/\omega_p = 0.00253$ and $v_{\mathrm{F}}/c = 0.0046$ (see Ref. [59]).

There are several ways to define L_{eff} for nanoshells [60, 61], however intuitive and simple approach $L_{\mathrm{eff}} = l_i$ gives acceptable and even negligible error [18]. Therefore eq. (7) can be written in the form:

$$\gamma_{\mathrm{fin}} = \gamma_{\mathrm{bulk}} + \frac{k v_{\mathrm{F}}}{\rho - \rho \sqrt[3]{f_{i,i+1}}}. \quad (8)$$

Hence, taking into account equations (6) and (8), the dielectric permittivity of thin metallic layers becomes function of size parameter ρ and filling factors $f_{i,i+1}$. For example, in the case of two-layered Au nanoshell, equation (5) becomes implicit function:

$$f_{12} = \frac{\overline{\varepsilon}_1 + 2\overline{\varepsilon}_2(f_{12}, \rho)}{\overline{\varepsilon}_1 - \overline{\varepsilon}_2(f_{12}, \rho)} \frac{\overline{\varepsilon}_{\mathrm{IA}}(\rho) - \overline{\varepsilon}_2(f_{12}, \rho)}{\overline{\varepsilon}_{\mathrm{IA}}(\rho) + 2\overline{\varepsilon}_2(f_{12}, \rho)}. \quad (9)$$

Therefore the IA condition becomes more complicated: $\overline{\varepsilon}_{\mathrm{av}}^{(2)}(f_{12}, \rho) \equiv \overline{\varepsilon}_{\mathrm{IA}}(\rho)$ and $\overline{\varepsilon}_{\mathrm{av}}^{(3)}(f_{12}, f_{23}, \rho) \equiv \overline{\varepsilon}_{\mathrm{IA}}(\rho)$ for two- and three-layered nanoparticles, respectively.

2.4. Absorption Spectra

We employ the Mie theory [62] with expansions for two- and three-layered spherical nanoparticles [58, 63] to calculate the absorption efficiency

$$Q_a(\lambda) = \sigma_a(\lambda)/\pi R^2. \quad (10)$$

We take into account multipoles with up to $n = 1000$ order in both cases, i.e. the absorption spectra are calculated with high accuracy.
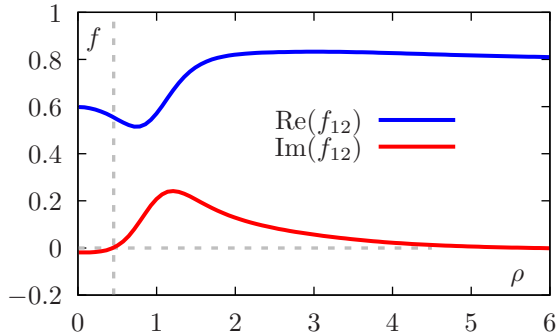
5

Figure 2: (Color online) Real $\mathrm{Re}\left[f_{12}(\rho)\right]$ and imaginary $\mathrm{Im}\left[f_{12}(\rho)\right]$ parts of the filling factor $f_{12}(\rho)$ (eq. (5)) for Si/Au nanoshells excited by an incident radiation with the wavelength $\lambda = 750\mathrm{nm}$ disregarding QSE.

3. Results

3.1. Ideal Absorption of Nanoshells

We start with the definition of IA conditions for two-layered Si/Au nanoshells. We assume that nanoparticles are embedded in homogeneous environment with $\varepsilon_{\mathrm{b}} = 1.78$. The dielectric permittivity $\varepsilon_2(\lambda)$ of gold was taken from Ref. [64]

Fig. 2 shows $\mathrm{Re}\left[f_{12}(\rho)\right]$ and $\mathrm{Im}\left[f_{12}(\rho)\right]$ as functions of the size parameter ρ at the wavelength $\lambda = 750\mathrm{nm}$ without taking into consideration QSE (see eq. (5)). It is clearly seen that the condition $\mathrm{Im}\left[f_{12}(\rho)\right] \equiv 0$ is met twice. In the first case we have $\rho = 0.45$ and $\mathrm{Re}(f_{12}) = 0.555$, while in the second case there are a set of ρ for whose $\mathrm{Im}\left[f_{12}(\rho)\right] = 0$. However in the second case $\rho > 5.5$, which does not meet the requirements for biomedical applications, because total particle size is too large. Similar dependency takes place for Au nanoshells with other core materials: the condition $\mathrm{Im}\left[f_{12}(\rho)\right] = 0$ is met twice and in the second case, the size of nanoshells are generally comparable or even larger then the wavelength of incident
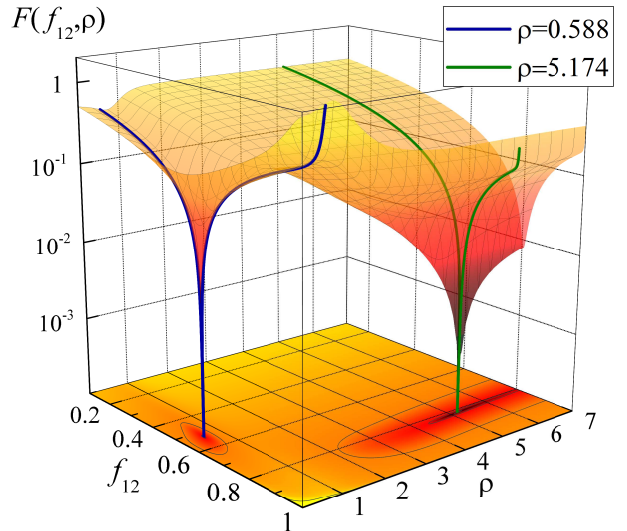

Figure 3: (Color online) The function $F(f_{12},\rho) = |\overline{\varepsilon}_{\mathrm{av}}^{(2)}(f_{12},\rho) - \overline{\varepsilon}_{\mathrm{IA}}(\rho)|$ for Si/Au nanoshells excited by incident radiation with the wavelength $\lambda = 750\mathrm{nm}$ taking into account QSE. Solid lines represent cut views: $F(f_{12}, 0.588)$ (blue line) and $F(f_{12}, 5.174)$ (green line).

radiation. Therefore we will not include data for two-layered nanoshells with $2R \simeq \lambda$ to our paper.

Next, consider the same physical problem but taking into account QSE. Fig. 3 shows the function $F(f_{12},\rho) = |\overline{\varepsilon}_{\mathrm{av}}^{(2)}(f_{12},\rho) - \overline{\varepsilon}_{\mathrm{IA}}(\rho)|$ for the same conditions as in Fig. 2. It can be seen that there are similarly two pairs $\{f_{12},\rho\}$ satisfying IA condition $\overline{\varepsilon}_{\mathrm{av}}^{(2)} = \overline{\varepsilon}_{\mathrm{IA}}$, namely: $\{0.529, 0.588\}$ and $\{0.817, 5.174\}$. Similarly, this feature will take place for the nanoshells with other cores. However, we will consider only the case $\rho \leq 1$. Thus, one can find IA conditions for any nano-shell structures at the required radiation wavelength using the above procedures both taking into account QSE and disregarding it.

Fig. 4a shows the spectral dependence of parameters ρ and f_{12} for IA of Si/Au nanoshells with IA. It
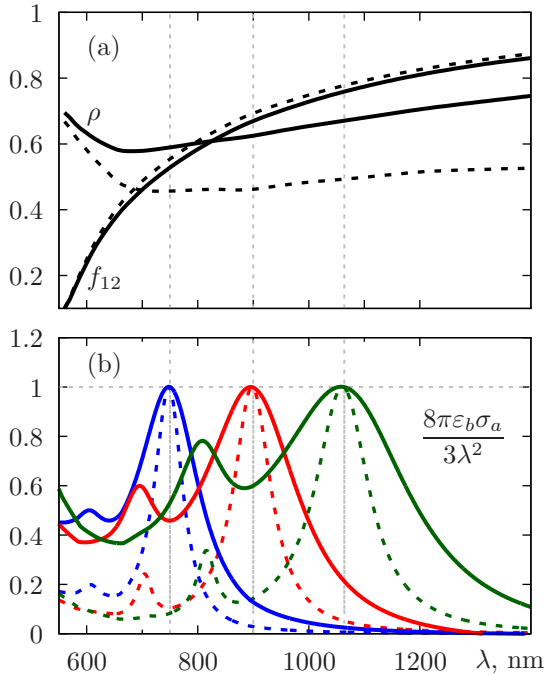
Figure 4: (Color online) (a) The spectral dependence of the filling factor f_{12} and the size parameter ρ for Si/Au nanoshells and (b) the dimensionless absorption spectra, $8\pi\varepsilon_b\sigma_a/(3\lambda^2)$, for Si/Au nanoshells calculated for 3 different pairs of values ρ and f_{12} providing IA at several wavelengths: 750nm, 900nm and 1064nm. Data presented for both disregarding and taking into account QSE: dashed and solid lines, respectively.

is clearly shown that QSE play a crucial role for determining the geometrical parameters of ideally absorbing nanoshells. Thus, taking into account these effects, the radius of nanoshell becomes ≈ 1.3 times larger compared to the case disregarding them for $\lambda > 700$nm. However the filling factor f_{12} remains nearly the same in both cases.

The dimensionless absorption spectra for several types of IA structures of Si/Au nanoshells are shown in Fig. 4b. We have selected three pairs of parameters $\{f_{12}, \rho\}$ to reach the IA conditions at wavelengths that correspond to working frequen-
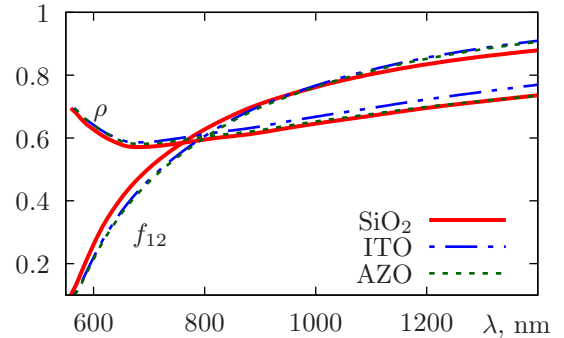

Figure 5: (Color online) The spectral dependence of the filling factor f_{12} and the size parameter ρ for x/Au nanoshells with different core materials: SiO$_2$; ITO; AZO. Calculations performed taking into account QSE.

cies of widely used medical lasers: $\lambda_1 = 750$nm (Alexandrite laser); $\lambda_2 = 900$nm (GaAs laser) and $\lambda_3 = 1064$nm (Nd:YAG laser). It can be easily seen that condition (3) is satisfied for chosen geometrical parameters at desired wavelengths. Indeed, the peak values of $8\pi\varepsilon_b\sigma_a/(3\lambda^2)$ equal unity for both cases of including and disregarding QSE. However, absorption spectra are noticeably broaden in the case of taking into consideration QSE compared to the case of neglecting it. Despite the fact that the peak values of dimensionless absorption $8\pi\varepsilon_b\sigma_a/(3\lambda^2)$ are the same in both cases, the maximum values of absorption efficiency $Q_a = \sigma_a/\pi R^2$ drop about 1.7 times in the case of including of QSE because of increased value of size parameter $\rho = kR$.

From Fig. 4 we can conclude that QSE are significant for determining both IA conditions and absorption spectra for Au nanoshells. Therefore in further studies of IA we do not ignore finite size effects in the paper.

Now we turn to consideration of nanoshells with other core materials. The goal is to test alternative
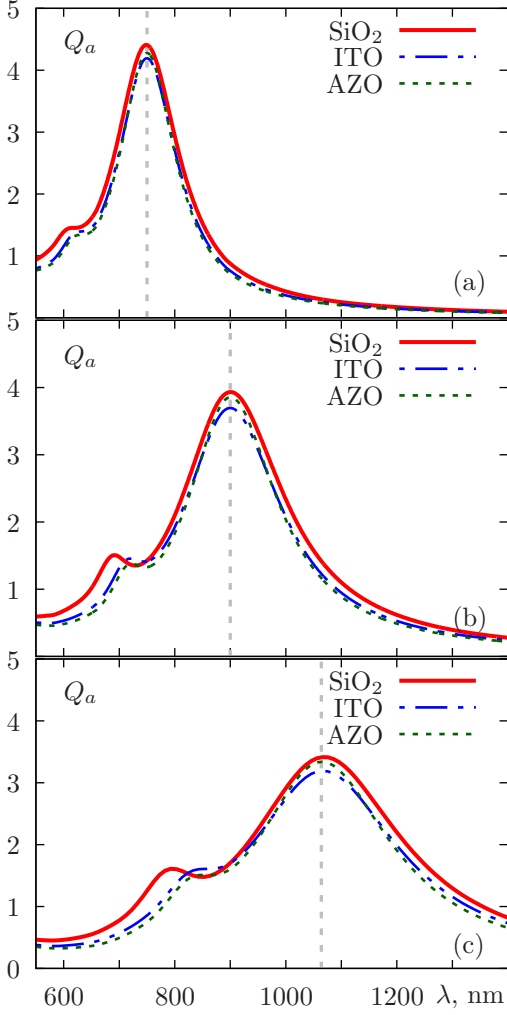
Figure 6: (Color online) The absorption spectra for x/Au nanoshells with different cores: SiO_2; ITO; AZO. Calculations are made with taking into account QSE and for 3 different pairs $\{\rho, f_{12}\}$ providing ideal absorption at several wavelengths: (a) 750nm; (b) 900nm and (c) 1064nm.

plasmonic materials for biomedical applications and to compare them with well-known material such as SiO_2 which is widely used for these applications. To this end we have calculated size characteristics (Fig. 5) and corresponding spectra (Fig. 6) for SiO_2/Au, ITO/Au and AZO/Au nanoshells.

It can be easily seen that curves in Fig. 5 are slightly differ from corresponding curves in Fig. 4.

Moreover, size parameter ρ and filling factor f_{12} are nearly the same for different core materials in Fig. 5. However ITO/Au nanoshells provide IA conditions with larger values of size parameter ρ. Finally, size characteristics and absorption spectra of GZO/Au and ZnO/Au nanoshells are same as for AZO/Au nanoparticles (data not shown).

Fig. 6 shows that absorption spectra of x/Au nanoshells with IA structures are similar for different core materials. However for large values of size parameter ρ the difference becomes more pronounced (Fig. 6c) and Si/Au nanoshells exhibit slightly better resonant properties. Nevertheless the total amount of absorbed energy is the same in all cases and satisfy eq. (3) for the dipole mode.

3.2. Ideal Absorption of Nanomatryoshkas

In this section we consider IA structure for three-layered Au/x/Au nanomatryoshkas with different intermediate layers. All calculations are performed taking into consideration QSE for nanoparticles embedded in water with $\varepsilon_b = 1.78$.

Search for size characteristics of ideally absorbing nanomatryoshkas is carried out in a following way. We determine parameters $\{f_{12}, f_{23}, \rho\}$ by finding local minimum of function $F(f_{12}, f_{23}, \rho) = |\overline{\varepsilon}_{av}^{(3)}(f_{12}, f_{23}, \rho) - \overline{\varepsilon}_{IA}(\rho)|$ for a given wavelength λ. There are several IA designs for nanomatryoshkas, however we consider only nanoparticles with $\rho < 1$.

Size characteristics of nanomatryoshkas providing IA at selected wavelengths are shown in table 1. It should be noticed that size parameter ρ and thickness l_3 of outer Au layer are similar for two-layered and three-layered nanoparticles at given wavelengths. We emphasize that $l_3 < 12$nm
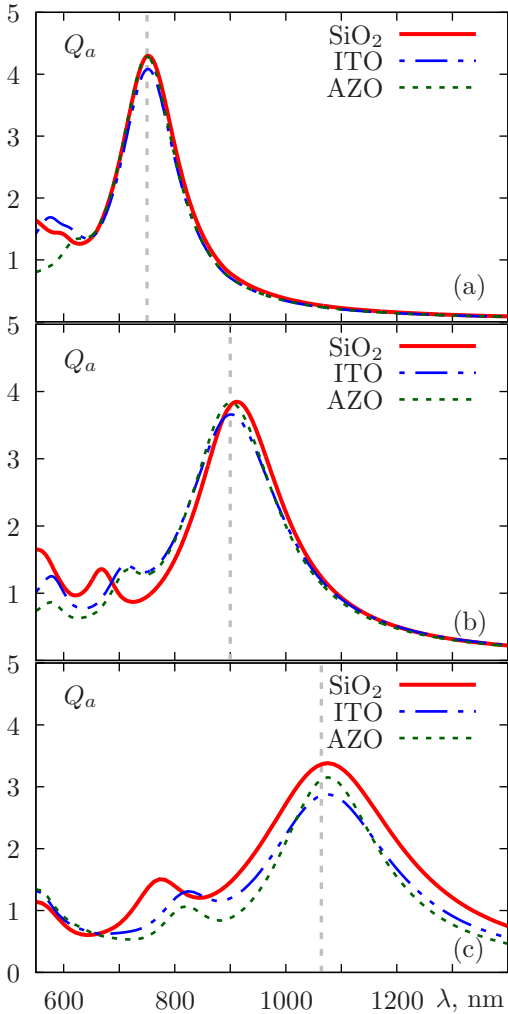
Figure 7: (Color online) The absorption spectra for Au/x/Au nanomatryoshkas with different intermediate layers: SiO$_2$; ITO; AZO. Calculations are performed with taking into account QSE for three different combinations $\{\rho, f_{12}, f_{23}\}$ providing ideal absorption at several wavelengths: (a) 750nm; (b) 900nm and (c) 1064nm.

in all cases for nanomatryoshkas, which leads to manifestation of QSE.

Corresponding spectra for Au/x/Au nanomatryoshkas are shown in Fig. 7. We can see that IA spectra for nanomartyoshkas are similar with corresponding spectra of nanoshells at the same wavelengths. However large nanoparticles exhibit

slightly worse resonant properties for Au/ITO/Au and Au/AZO/Au configurations at $\lambda = 1064$nm (see Fig. 7c).

Recently it was shown [65] that three-layered nanoparticles can exhibit superabsorption (SA) phenomenon, for which the absorption cross-section σ_a is higher than the theoretical limit in eq. (3). We remind here that the IA limits cannot be surpassed in a given multipole channel while SA phenomenon is referred to surpassing the IA limit of a single multipole mode by multimode absorption [65]. We examined Au/x/Au nanomatryoshkas for the SA conditions at wavelengths corresponding to Fig. 7. Calculations show that the IA limit is exceeded by $\approx 2\%$ which is mostly related to computational accuracy rather than to enhanced multimode absorption.

Finally, ideally absorbing nanoparticles whose geometries were predicted using dipole equivalence principle for two- and three- layered nanoparticles (eqs. (1) and (2), correspondingly), provide absorption spectra (calculated using exact Mie theory expansions with taking into account high order multipoles, eq. (10)) which perfectly fits to predicted wavelength. Therefore, we can state that dipole equivalence principle still works for large, up to ≈ 170nm diameter multilayered nanoparticles considered in this paper. In this case, higher multipoles contribution is negligibly small compared to the electric dipole.

4. Conclusion

In this paper we have determined the conditions for reaching the ideal absorption of plasmonic

Table 1: Size characteristics of nanoshells and nanomatryoshkas providing IA at several wavelengths taking into account QSE. Thicknesses l_1/l_2 and $l_1/l_2/l_3$ are given in nanometers. Deviation from l_i within $5-10\%$ insignificantly affects the absorption spectra.

Configuration	$\lambda = 750$nm	$\lambda = 900$nm	$\lambda = 1064$nm
Si/Au	42.6/10.1	58.7/9.4	77.7/7.5
SiO$_2$/Au	43.3/8.8	59.1/7.2	77.7/6.3
AZO/Au	43.1/9.9	59.6/7.6	78.6/6.2
GZO/Au	44.0/9.1	61.0/7.0	80.9/5.4
ITO/Au	43.7/9.8	60.8/7.6	80.8/6.1
ZnO/Au	42.3/9.7	58.6/8.7	77.7/7.7
Au/Si/Au	14.8/27.8/11.0	20.9/37.8/9.1	30.6/47.2/8.2
Au/SiO$_2$/Au	19.0/24.0/9.9	32.1/26.8/8.7	35.0/42.8/7.0
Au/AZO/Au	5.4/37.6/9.9	13.6/45.9/7.7	47.3/32.4/7.7
Au/GZO/Au	15.0/29.2/9.7	34.5/27.6/8.3	35.5/46.2/5.7
Au/ITO/Au	14.2/29.6/10.5	18.7/42.2/7.9	49.5/34.2/7.8
Au/ZnO/Au	13.0/29.4/11.6	18.2/40.4/9.3	25.2/52.6/8.2

nanoshells and nanomatryoshkas with outer Au layers for near infrared wavelength range. Search method of IA structures proposed in Ref. [1] was modified by taking into account QSE for thin metallic layers. It was shown that quantum finite size effects play crucial role for determining IA conditions for Au coatings. Namely, the size parameter ρ increases by factor ≈ 1.3 and filling factor f_{12} remains almost unchanged compared to the case of disregarding QSE for nanoshells.

The obtained results show that alternative plasmonic materials (AZO, GZO, ITO) in multilayered Au structures can be used for PPTT. We have shown that such nanoparticles exhibit similar optical properties as other types of nanoparticles: Si/Au, SiO$_2$/Au and Au/SiO$_2$/Au nanospheres. Despite the fact that nanoparticles containing al-

ternative plasmonic materials do not reveal significantly better resonant properties, utilizing of alternative plasmonic materials in PPTT can be promising due to their high thermal conductivity [66, 67] that allows one to apply lower radiation intensity for hyperthermia of malignant cells that does not affect normal cells.

It should be noticed that there are still no state of the art technologies for fabrication of monodisperse nanoparticles considered in this paper, and creation of such technologies is a challenge for close future. Let us also note that our calculations show, that even $5-10\%$ deviation from l_i (see table 1) does not significantly change the absorption spectra of nanoparticles. For stronger polydispersity, the absorption peak of individual nanoparticles will considerably shift to longer or shorter wavelengths.

This effect will lead to the broadening of colloid absorption spectra. However, the position of maximum in absorption spectrum of colloid will not change.

Finally, x/Au and Au/x/Au spherical nanoparticles with IA have similar overall sizes and optical properties for the same "x" materials. Therefore, for reaching the maximum values of absorbed radiation energy, nanoshells with IA seem to be preferable in biomedical applications due to ease of fabrication compared to nanomatryoshkas.

5. Acknowledgements

[1] V. Grigoriev, N. Bonod, J. Wenger, B. Stout, Optimizing nanoparticle designs for ideal absorption of light, ACS Phot. 2 (2) (2015) 263–270.

[2] G. V. Naik, V. M. Shalaev, A. Boltasseva, Alternative plasmonic materials: Beyond gold and silver, Adv. Mater. 25 (24) (2013) 3264–3294.

[3] M. I. Stockman, Nanoplasmonics: past, present, and glimpse into the future, Opt. Express 19 (2011) 22029.

[4] A. Kuznetsov, A. Miroshnichenko, Y. Fu, J. Zhang, B. Lukyanchuk, Magnetic light, Scientific Reports 2 (2012) 492.

[5] A. B. Evlyukhin, S. M. Novikov, U. Zywietz, R. L. Eriksen, C. Reinhardt, S. I. Bozhevolnyi, B. N. Chichkov, Demonstration of magnetic dipole resonances of dielectric nanospheres in the visible region, Nano Letters 12 (7) (2012) 3749–3755.

[6] N. G. Khlebtsov, A. G. Melnikov, L. A. Dykman, V. A. Bogatyrev, Photopolarimetry in remote sensing, Kluwer Academic Pub., 2004, Ch. Optical properties and biomedical applications of nanostructures based on gold and silver bioconjugates, pp. 1–44.

[7] C. Loo, L. Hirsch, M. Lee, E. Chang, I. West, N. Halas, R. Drezek, Gold nanoshell bioconjugates for molecular imaging in living cells, Opt. Lett. 30 (9) (2005) 1012–1014.

[8] N. Rosi, C. Mirkin, Nanostructures in biodiagnostics, Chem. Rev. 105 (4) (2005) 1547–1562.

[9] D. Stuart, A. Haes, C. Yonzon, E. Hicks, R. Van Duyne, Biological applications of localised surface plasmonic phenomenae, IEE Proceedings - Nanobiotechnology 152 (1) (2005) 13–32.

[10] M. M. Cheng, G. Cuda, Y. L. Bunimovich, M. Gaspari, J. R. Heath, H. D. Hill, C. A. Mirkin, A. J. Nijdam, R. Terracciano, T. Thundat, M. Ferrari, Nanotechnologies for biomolecular detection and medical diagnostics, Current Opinion in Chemical Biology 10 (1) (2006) 11–19.

[11] X. Huang, I. El-Sayed, W. Qian, M. El-Sayed, Cancer cell imaging and photothermal therapy in the near-infrared region by using gold nanorods, J. Am. Chem. Soc. 128 (6) (2006) 2115–2120.

[12] B. Khlebtsov, V. Zharov, A. Melnikov, V. Tuchin, N. Khlebtsov, Optical amplification of photothermal therapy with gold nanoparticles and nanoclusters, Nanotechnology 17 (20) (2006) 5167.

[13] J. Lakowicz, Plasmonics in biology and plasmon-controlled fluorescence, Plasmonics 1 (1) (2006) 5–33.

[14] G. Paciotti, D. Kingston, T. L., Colloidal gold nanoparticles: a novel nanoparticle platform for developing multifunctional tumor-targeted drug delivery vectors, Drug Development Research 67 (1) (2006) 47–54.

[15] D. Pissuwan, S. Valenzuela, M. Cortie, Therapeutic possibilities of plasmonically heated gold nanoparticles, Trends Biotechnol. 24 (2) (2006) 62–67.

[16] A. Wei, Designing plasmonic nanomaterials as sensors of biochemical transport, e-Journal of Surface Science and Nanotechnology 4 (2006) 9–18.

[17] P. Jain, I. El-Sayed, M. El-Sayed, Au nanoparticles target cancer, Nano Today 2 (1) (2007) 18–29.

[18] B. N. Khlebtsov, N. G. Khelbtsov, Biosensing potential of silica/gold nanoshells: Sensitivity of plasmon resonance to the local dielectric environment, J. Quant. Spectrosc. Radiat. Transfer 106 (1-3) (2007) 154169.

[19] S. Kumar, N. Harrison, R. Richards-Kortum, K. Sokolov, Plasmonic nanosensors for imaging intracellular biomarkers in live cells, Nano Letters 7 (5) (2007) 1338–1343.

[20] N. Khlebtsov, Optics and biophotonics of nanoparticles with a plasmon resonance, Quantum Electronics 38 (6) (2008) 504–529.

[21] M. Stewart, C. Anderton, L. Thompson, I. Maria, S. Gray, J. Rogers, R. Nuzzo, Nanostructured plasmonic sensors, Chem. Rev. 108 (2) (2008) 494–521.

[22] N. Khlebtsov, L. A. Dykman, Optical properties and biomedical applications of plasmonic nanoparticles, J. Quant. Spectrosc. Radiat. Transfer 111 (1) (2010) 1–35.

[23] J. Kim, S. Park, J. Lee, S. Jin, J. Lee, I. Lee, I. Yang, J.-S. Kim, S. K. Kim, M. Cho, T. Hyeon, Designed fabrication of multifunctional magnetic gold nanoshells and their application to magnetic resonance imaging and photothermal therapy, Angewandte Chemie International Edition 45 (46) (2006) 7754–7758.

[24] I. Maksimova, G. Akchurin, B. Khlebtsov, G. Terentyuk, G. Akchurin, I. Ermolaev, A. Skaptsov, E. Soboleva, N. Khlebtsov, V. Tuchin, Near-infrared laser photothermal therapy of cancer by using gold nanoparticles: Computer simulations and experiment, Medical Laser Application 22 (3) (2007) 199–206.

[25] E. B. Dickerson, E. Dreaden, X. Huang, I. El-Sayed, H. Chu, S. Pushpanketh, J. McDonald, M. El-Sayed, Gold nanorod assisted near-infrared plasmonic photothermal therapy (pptt) of squamous cell carcinoma in mice, Cancer Letters 269 (1) (2008) 57–66.

[26] X. Huang, P. Jain, I. El-Sayed, M. El-Sayed, Plasmonic photothermal therapy (pptt) using gold nanoparticles, Lasers Med. Sci. 23 (3) (2008) 217–228.

[27] D. Lapotko, Therapy with gold nanoparticles and lasers: what really kills the cells?, Nanomedicine 4 (3) (2009) 253–256.

[28] G. Terentyuk, G. Maslyakova, L. Suleymanova, N. Khlebtsov, B. Khlebtsov, G. Akchurin, I. Maksimova, V. Tuchin, Laser-induced tissue hyperthermia mediated by gold nanoparticles: toward cancer phototherapy, J. Biomed. Opt. 14 (2) (2009) 021016.

[29] E. Lukianova-Hleb, Y. Hu, L. Latterini, L. Tarpani, S. Lee, R. Drezek, Plasmonic nanobubbles as transient vapor nanobubbles generated around plasmonic nanoparticles, ACS Nano 4 (4) (2010) 2109–2123.

[30] X. Huang, M. El-Sayed, Plasmonic photo-thermal therapy (pptt), Alexandria Journal of Medicine 47 (1) (2011) 1–9.

[31] H. Liu, D. Chen, L. Li, T. Liu, L. Tan, X. Wu, , F. Tang, Multifunctional gold nanoshells on silica nanorattles: A platform for the combination of photothermal therapy and chemotherapy with low systemic toxicity, Angew. Chem. 50 (54) (2011) 891–895.

[32] C. Ayala-Orozco, C. Urban, M. Knight, A. Urban, O. Neumann, S. Bishnoi, S. Mukherjee, A. Goodman, H. Charron, T. Mitchell, M. Shea, R. Roy, S. Nanda, R. Schiff, N. Halas, A. Joshi, Au nanomatryoshkas as efficient near-infrared photothermal transducers for cancer treatment: Benchmarking against nanoshells, ACS Nano 8 (6) (2014) 6372–6381.

[33] J. Zhang, B. Liu, H. Liu, X. Zhang, W. Tan, Aptamer-conjugated gold nanoparticles for bioanalysis, Nanomedicine 8 (6) (2013) 983–993.

[34] C. Reinemann, B. Strehlitz, Aptamer-modified nanoparticles and their use in cancer diagnostics and treatment, Swiss Med Wkly 144 (2014) 13908.

[35] I. El-Sayed, X. Huang, M. El-Sayed, Surface plasmon resonance scattering and absorption of anti-egfr antibody conjugated gold nanoparticles in cancer diagnostics: applications in oral cancer, Nano Letters 5 (5) (2005) 829–834.

[36] I. El-Sayed, X. Huang, M. El-Sayed, Selective laser photo-thermal therapy of epithelial carcinoma using anti-egfr antibody conjugated gold nanoparticles, Cancer Letters 239 (1) (2006) 129–135.

[37] X. Huang, P. Jain, I. El-Sayed, M. El-Sayed, Determination of the minimum temperature required for selective photothermal destruction of cancer cells using immunotargeted gold nanoparticles, Photochem. Photobiol. 82 (2) (2006) 412–417.

[38] M. Mackey, M. R. K. Ali, L. A. Austin, R. D. Near, M. A. El-Sayed, The most effective gold nanorod size for

plasmonic photothermal therapy: Theory and in vitro experiments, J. Phys. Chem. B 118 (5) (2014) 1319–1326.

[39] C. Loo, A. Lowery, N. Halas, J. West, R. Drezek, Immunotargeted nanoshells for integrated cancer imaging and therapy, Nano Letters 5 (4) (2005) 709–711.

[40] L. Hirsch, A. Gobin, A. Lowery, F. Tam, R. Drezek, N. Halas, J. West, Metal nanoshells, Annals. Biomed. Eng. 34 (1) (2006) 15–22.

[41] D. J. Wu, X. D. Xu, X. J. Liu, Influence of dielectric core, embedding medium and size on the optical properties of gold nanoshells, Solid State Comm. 146 (1-2) (2008) 7–11.

[42] J. J. Penninkhof, A. Moroz, A. van Blaaderen, A. Polman, Optical properties of spherical and oblate spheroidal gold shell colloids, J. Phys. Chem. C 112 (11) (2008) 4146–4150.

[43] T. A. Erickson, J. W. Tunnell, Mixed Metal Nanomaterials, Wiley-VCH, Weinheim, 2009, Ch. Gold Nanoshells in Biomedical Applications, pp. 1–44.

[44] C. Ayala-Orozco, C. Urban, S. Bishnoi, A. Urban, H. Charron, T. Mitchell, M. Shea, S. Nanda, R. Schiff, N. Halas, A. Joshi, Sub-100 nm gold nanomatryoshkas improve photo-thermal therapy efficacy in large and highly aggressive triple negative breast tumors, Journal of Controlled Release 191 (2014) 90 – 97.

[45] J. Chen, D. Wang, J. Xi, L. Au, A. Siekkinen, A. Warsen, Z. Li, H. Zhang, Y. Xia, X. Li, Immuno gold nanocages with tailored optical properties for targeted photothermal destruction of cancer cells, Nano Letters 7 (5) (2007) 1318–1322.

[46] S. Wang, P. Huang, L. Nie, R. Xing, D. Liu, Z. Wang, J. Lin, S. Chen, G. Niu, G. amd Lu, X. Chen, Single continuous wave laser induced photodynamic/plasmonic photothermal therapy using photosensitizer-functionalized gold nanostars, Adv. Mater. 25 (22) (2013) 3055–3061.

[47] J. Z. Zhang, Biomedical applications of shape-controlled plasmonic nanostructures: A case study of hollow gold nanospheres for photothermal ablation therapy of cancer, J. Phys. Chem. Lett. 1 (4) (2010) 686–695.

[48] V. S. Gerasimov, A. E. Ershov, S. V. Karpov, S. P. Polyutov, P. N. Semina, Optimization of photothermal methods for laser hyperthermia of malignant cells using bioconjugates of gold nanoparticles, Colloid J. 78 (4) (2016) 435–442.

[49] R. Kannadorai, Q. Liu, Optimization in interstitial plasmonic photothermal therapy for treatment planning, Med. Phys. 40 (10) (2013) 103301.

[50] M. Tribelsky, Anomalous light absorption by small particles, Europhys. Lett. 94 (1) (2011) 14004.

[51] R. Fleury, J. Soric, A. Alu, Physical bounds on absorption and scattering for cloaked sensors, Phys. Rev. B 89 (4) (2014) 045122.

[52] O. D. Miller, C. W. Hsu, M. T. H. Reid, W. Qiu, B. G. DeLacy, J. D. Joannopoulos, M. Soljai, S. G. Johnson, Fundamental limits to extinction by metallic nanoparticles, Phys. Rev. Lett. 112 (2014) 123903.

[53] S. Tretyakov, Maximizing absorption and scattering by dipole particles, Plasmonics 9 (4) (2014) 935–944.

[54] H. Zhou, I. Honma, H. Komiyama, Controlled synthesis and quantum-size effect in gold-coated nanoparticles, Phys. Rev. B 50 (16) (1994) 12052.

[55] D. C. Look, K. D. Leedy, Zno plasmonics for telecommunications, Appl. Phys. Lett. 102 (18) (2013) 182107.

[56] D. C. Look, K. D. Leedy, D. B. Thomson, B. Wang, Defects in highly conductive zno for transparent electrodes and plasmonics, J. Appl. Phys. 115 (1) (2014) 012002.

[57] M. K. Hamza, J.-M. Bluet, K. Masenelli-Varlot, B. Canut, O. Boisron, P. Melinon, B. Masenelli, Tunable mid ir plasmon in gzo nanocrystals, Nanoscale 7 (2015) 12030–12037.

[58] C. F. Bohren, D. R. Huffman, Absorption and Scattering of Light by Small Particles, John Wiley & Sons, New York, 1998.

[59] U. Kreibig, M. Vollmer, Optical Properties of Metal Clusters, Springer-Verlag, Berlin, 1995.

[60] C. G. Granqvist, O. Hunderi, Optical absorption of ultrafine metal spheres with dielectric cores, Zeitschrift für Physik B Condensed Matter 30 (1) (1978) 47–51.

[61] S. M. Kachan, A. N. Ponyavina, Resonance absorption spectra of composites containing metal-coated nanoparticles, Journal of Molecular Structure 563-564 (2001) 267–272.

[62] G. Mie, Beitrage zur optik truber medien, speziell kolloidaler metallosungen, Ann. Physik 330 (1908) 377–445.

[63] Z. S. Wu, Y. P. Wang, Electromagnetic scattering for multilayered sphere: Recursive algorithms, Radio Science 26 (6) (1991) 1393–1401.

[64] P. B. Johnson, R. W. Christy, Optical constants of the noble metals, Phys. Rev. B 6 (12) (1972) 4370–4379.

[65] K. Ladutenko, P. Belov, O. Pena-Rodriguez, A. Mirzaei, A. Miroshnichenko, I. Shadrivov, Superabsorption of light by nanoparticles, Nanoscale 7 (45) (2015) 18897–901.

[66] Y. Fujishiro, M. Miyata, M. Awano, K. Maeda, Effect of microstructural control on thermoelectric properties of hot-pressed aluminum-doped zinc oxide, J. Am. Ceram. Soc. 86 (12) (2003) 2063–2066.

[67] T. Yagi, K. Tamano, Y. Sato, N. Taketoshi, T. Baba, Y. Shigesato, Analysis on thermal properties of tin doped indium oxide films by picosecond thermoreflectance measurement, J. Vac. Sci. Technol. A 23 (4) (2005) 1180–1186.